CFD Letters

Journal homepage:
https://semarakilmu.com.my/journals/index.php/CFD_Letters/index
ISSN: 2180-1363

Free-Surface Vortices Mitigation using Anti-Vortex Plates in Dam Intakes through CFD

Thiennieesh Manogaran[1], Mohd Remy Rozainy Mohd Arif Zainol[1,2,*], Muhammad Khairi A. Wahab[1] Mohd Sharizal Abdul Aziz[3], Nurhanani Abd Aziz[4], Nazirul Mubin Zahari[4], Mohd Hafiz Zawawi[4], Mohd Rashid Mohd Radzi[5]

[1] School of Civil Engineering, Engineering Campus, Universiti Sains Malaysia (USM), 14300 Nibong Tebal, Malaysia
[2] River Engineering And Urban Drainage Research Institute (REDAC), Engineering Campus, Universiti Sains Malaysia (USM), 14300 Nibong Tebal, Malaysia
[3] School of Mechanical Engineering, Engineering Campus, Universiti Sains Malaysia (USM), 14300 Nibong Tebal, Malaysia
[4] Department of Civil Engineering, College of Engineering, Universiti Tenaga Nasional (UNITEN), 43000 Kajang, Selangor, Malaysia
[5] Hydro Life Extension Program (HELP), Business Development (Asset) Unit, TNB Power Generation Division, 46050 Petaling Jaya, Selangor, Malaysia

ARTICLE INFO

Article history:
Received 8 October 2022
Received in revised form 10 November 2022
Accepted 9 December 2022
Available online 1 June 2023

Keywords:
Dam Modelling; Free-Surface Vortices; Flow Characteristics; Anti-Vortex Plates; Disaster

ABSTRACT

By recording parameters such as velocity and volume fraction by contour plots or plane, a CFD model enables to analyse flow patterns in the model, such as free-surface vortices A free-surface vortex, a common problem may indeed be observed in a variety of submerged water intakes, notably shallow basins and low head intakes. These FSVs are likely to form an air-core vortex, eventually entrapping detritus and air pockets in the water intake system and causing further vibration and damage to the downstream turbine. When paired with a high velocity, the formation of vortices in the system been known to produce hydraulic transients, which cause unwanted operation or pressure changes. The model of the 1:100 scale dam reservoir was generated, computationally meshed, and modelled in FLUENT under ANSYS 2019 R3 at two different water levels to observe the FSV formations. To mitigate those FSV formations, anti-vortex plates with two distinct plates—square and wedge—were used. From the findings square plates outperform wedge plates because square it lowers the speed of a fast-flowing fluid and reduces it into a laminar flow rather of a turbulent flow, which benefits vortex class deterioration. Data from the simulation and experimental shows a strong agreement in terms of velocity at outlet 1 from both water levels with relative errors of 3.0% and 14.1% respectively.

1. Introduction

Computational fluid dynamics, particularly employs numerical techniques and algorithms to solve fluid flow issues, is a subfield of fluid mechanics. In the past, scaled physical models were then constructed in hydraulic labs to study the flow, but they are expensive, time-consuming, and replete with issues because of scaling effects. Femtosecond computer simulations may now be used to

* *Corresponding author.*
E-mail address: ceremy@usm.my (Mohd Remy Rozainy Mohd Arif Zainol)

https://doi.org/10.37934/cfdl.15.6.2641

numerically study the performance of hydraulic structures as well as open channels in a reasonable amount of time and at a reasonable cost thanks to advancements in computer technology and more effective computational fluid dynamics (CFD) applications [1, 2]. With using approximations to solve partial differential equations (PDEs) regulating flows, computational fluid dynamics (CFD) has been shown to predict flow patterns. The method for evaluating how correctly the CFD model represents the actual environment from the perspective of the anticipated application is essential for its effectiveness. To give confidence in the expected results, CFD solutions must take into account the corresponding error ranges as well as uncertainties ensuing from the findings [3]. CFD is hugely beneficial for hydraulic engineering simply because it is typically more adaptable than a physical model in modifying the physical form and/or hydraulic conditions, enabling the testing of numerous configurations for comparison. In order to identify potential issues before creating the physical model, CFD may also be utilized as a component of the design process before creating an insignificant section of the hydraulic structure. By recording parameters such as velocity and volume fraction by contour plots or plane, a CFD model enables to analyze flow patterns in the model, such as free-surface vortices [4].

Free-surface vortex, a whirling flowing region revolving along a straight or curved axis, a common problem may indeed be observed in a variety of submerged water intakes, notably shallow basins and low head intakes. There are several different types of submerged water intakes, notably shallow basins and lower head intakes, where a free-surface vortex can form. Alden Research Laboratory was in charge of classifying free surface vortices. Their study led to the classification of vortices in to the six types, with type 1 vortices being the weakest and type 6 vortices being the strongest, as seen in Figure 1. Vortex type 1 (VT1), as resembles a cohesive swirl, has the least effect on hydraulic machinery; in contrast, VT6 coupled to a full air core has the most effect. Based on the vortices' intensity and growth, different categories were created. Some researchers have expanded this classification to include VT0 (i.e., no activity at this stage) [5-7]. Flow separation as well as eddy formation, asymmetrical approach conditions, a lack of critical submergence, an approach flow velocity higher exceeding 0.65 m/s, and an abrupt shift in flow direction are the leading factors [8]. These FSVs are likely to form an air-core vortex, eventually entrapping detritus and air pockets in the water intake system and causing further vibration and damage to the downstream turbine. When paired with a high velocity, the formation of vortices in the system been known to produce hydraulic transients, which cause unwanted operation or pressure changes [9, 10].

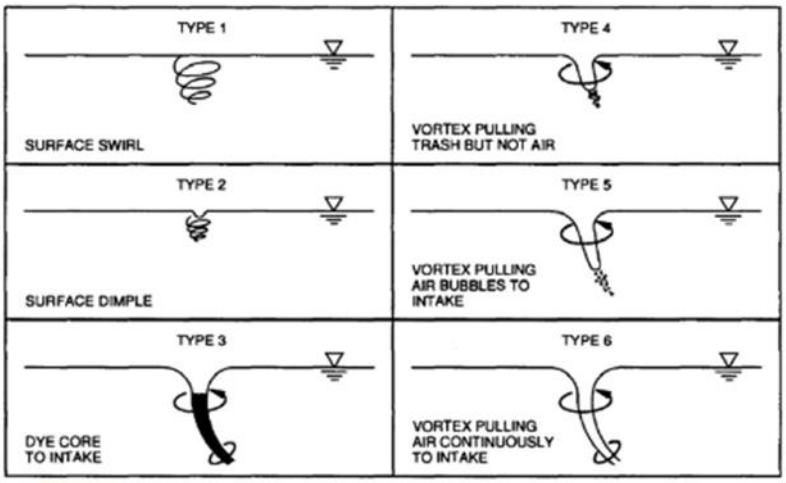

Fig. 1. Vortices classifications based on Alden Research Laboratory [11]

In order to mitigate these FSV formations, plates were used as anti-vortex device and the performance were studied as such in 2011, researchers conducted an experiment on the overall efficacy of horizontal perforated and solid plates placed on top of an intake for the suppression of surface vortex generation. The experiments were conducted out on the horizontal intake of the reservoir. It was found that both solid and perorated plates with 50% uniform openness with width ranging from 1 to 1.5D and length ranging from 1.5 to 2D eliminated all types of surface vortices at the intake. The value D is the intake diameter [12].

Using rectangular anti-vortex plates, a comprehensive set of studies was done in 2013 to partially reduce vortex intensity and air entrainment at vertical pipe intakes. The plates were employed alone and in pairs, and were symmetrically and asymmetrically arranged in relation to the pipe axis. According to the results, larger plates outperformed smaller plates when it was found that a dye core vortex, very weak air core vortex, and minor dimples were present. A complete air-core vortex that drew air bubbles towards the intake was seen for smaller plates. It was suggested to place the plates symmetrically as they are more effective in reducing vortex strength [13].

In 2014, the influence of plate dimensions on critical submergence was explored in an experimental model utilizing varying dimension of vertical plates with mesh. One of the most important design characteristics is the critical submergence (S_c) of the intake. In the case of insufficient critical submergence, the formation of a vortex at the dams causes air entrainment. As long as the intake submergence (S_i) is larger than the critical submergence ($S_i>S_c$), the rate of air entrainment is essentially zero. It was found that increasing the length of vertical plates is more efficient than raising the height of vertical plates in reducing the possibility of critical submergence [14].

A reservoir physical model was recently utilized to evaluate the performance of horizontal perforated plates in 2022. The performance of ten different types of perforated plates with varying dimensions, thicknesses, and mesh openings (i.e., 70%, 58% and 50%) was evaluated. Finally, it was determined that the effect of opening the plates to reduce vortex strength is greater than the size and thickness of the plates. The opening rate of the plates has a large effect on the vortex, and a 50% opening plate was able to dissipate all strong vortices [15].

Despite their benefits, anti-vortex plates have no design criteria. The design criterion for the size of solid and evenly perforated plates was experimentally obtained throughout the previous studies, taking into account the strength of surface vortices. Thus, the numerical performance of horizontal plates on dam intakes to reduce FSV generation is discussed in this article.

2. Methodology

2.1 Preparation of Numerical Model

Figure 2 depicts the model drawing of the 1:100 scale dam reservoir model with intake structures done in SolidWorks 2019 for this study. The geometry as in Figure 3 was then exported, computationally meshed, and modelled in FLUENT under ANSYS 2019 R3. The suggested dam model, as illustrated in Figure 2, is 5.9 meters long from upstream to downstream (reservoir to weir box) and 0.9 meters tall. The model starts with a rectangular box representing the upstream reservoir, which is then filled with landscape mimicking the dam prototype's on-site topography. As you approach the intake structure, the topology features uneven slopes and sharp edges. The intake structures then have four inlets that distribute reservoir water through four penstocks. At the downstream end of each penstock, four Francis turbine assemblies were connected. The spiral casing, stay vanes, guiding vanes, runner blades, and drafting tube are the main components. Because of its flexibility to operate

across a wide range of head and flow rate, the Francis turbine is the most often utilized reaction turbine type [16]. Each Francis turbine consists of 22 blades connected by a shaft as Figure 4.

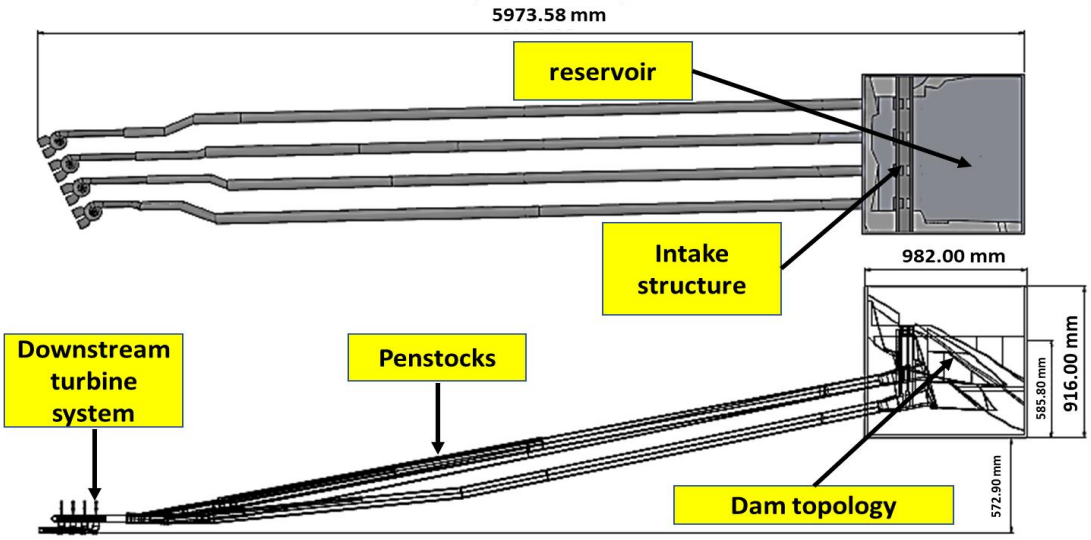

Fig. 2. Geometry drawing of dam model

Fig. 3. Computational domain of dam

Fig. 4. Francis turbine with dual outlet model

2.2 Numerical Methods and Features

2.2.1 Volume of fluid (VOF) with open channel flow

Using the VOF formulation and the open channel for volume fraction, ANSYS FLUENT can calculate the effects of open channel flow (such as water bodies, dams' components such as spillway and surface penetrating structures in unbounded streams). These flows require a free surface to exist between the fluid that is flowing and the fluid above it (generally the atmosphere). Gravity and inertia's forces often control flow. Each phase (fluid) is given a variable that represents the percentage of each computational cell that the phase occupies. This quantity is referred to as the "volume fraction of phase". In each computational cell, the volume fractions from all phases equal one. Common fields for all phases offer volume-averaged values for each variable and characteristic. For the mixing of all fluids, a unified momentum equation can be solved, and the subsequent velocity field is distributed by the phases [17, 18]. Both phases share the velocity field that results. Each control volume inside the domain is given the relevant characteristics and variables predicated upon given local value ($\boldsymbol{\alpha}_q$). The momentum and continuity equation for mixture is shown Eq. (1) and (2).

$$\frac{\partial(\rho\vec{u})}{\delta t} + \nabla\cdot(\rho\vec{u}\vec{u}) = -\nabla p + \nabla\left(\mu(\nabla\vec{u} + \nabla\vec{u}^T)\right) + \rho\vec{g} + \vec{T}_\sigma \tag{1}$$

$$\frac{\partial(\rho\vec{u})}{\delta t} + \nabla\cdot(\rho\vec{u}) = S \tag{2}$$

Where the density of mixture is ρ, μ is the viscosity of mixture, $\vec{u}$ is the initial velocity, and $\vec{T}_\sigma$ is the surface tension of the interphase. This multiphase model was applied for this simulation because, contingent on the volume fractions of relative phases in the cell, some variables and components in a given cell reflect group of individual phases or a mixture of phases. Topological changes are automatically taken into account by the level-set concept in VOF [19, 20]. Furthermore, because water surface is the point of contact between air and water, implementing boundary conditions here on surface has been disregarded. As a matter of fact, this method allows for unlimited water circulation at the interface [21, 22].

2.2.2 Standardized k- ε turbulence model

The most reliable method for simulating mean flow characteristics in turbulent flow scenarios is the k-epsilon (k) turbulence model. It is an equation-based model. In other words, it resolves two transport equations (PDEs) which thus take into consideration historical effects like convection as well as turbulent energy diffusion in additional to the conservation equations. The two conveyed variables are turbulent kinetic energy (k) where it determines the energy in turbulence, and turbulent dissipation rate (ε) relates to the rate at which turbulent kinetic energy is dissipated.

$$\frac{\partial\rho k}{\delta t} + \frac{\partial(\rho k u_i)}{\delta x_i} = \frac{\partial\alpha_f}{\delta x_j}\left[\frac{\mu_t}{\sigma_k}\frac{\partial_k}{\delta x_j}\right] + 2\mu_t E_{ij}E_{ij} - \rho\varepsilon \tag{3}$$

$$\frac{\partial(\rho\varepsilon)}{\delta t} + \frac{\partial(\rho\varepsilon u_i)}{\delta x_i} = \frac{\partial}{\delta x_j}\left[\frac{\mu_t}{\sigma_\varepsilon}\frac{\partial_\varepsilon}{\delta x_j}\right] + C_{1\varepsilon}2\mu_t E_{ij}E_{ij} - C_{2\varepsilon}\rho\frac{\varepsilon^2}{k} \tag{4}$$

Where u_i denotes the component of velocity with in corresponding direction, E_{ij} indicates a component of the rate of deformation and μ_t signifies eddy viscosity. A few variable constants are

also included in the equations. The values of these constants were established through numerous iterations of data incorporating for a variety of turbulent flows. These are as follows σ_k =1.00, σ_ε= 1.30, $C_{1\varepsilon}$= 1.44 and $C_{2\varepsilon}$ =1.92. The k- ε model is also precise and reliable for free-shear flows, such as those with minor pressure gradients [23]. The conventional k- ε turbulence model, which is based on a knowledge of the relevant dynamics, optimizes unknowns, and provides a set of axioms that can be used to a broad range of turbulent applications, is used as a result for a significantly practical approach.

2.2.3 SIMPLEC pressure-velocity coupling

ANSYS FLUENT has the SIMPLEC (SIMPLE-Consistent) method a pressure-predicated segregated algorithm which has the pressure correction under-relaxation factor set to 1.0 to avail in convergence speed [24]. The application of this modified correction equation has been found to expedite convergence in issues where pressure-velocity coupling is the primary impediment to finding a solution. Another serviceable aspect of SIMPLEC is the approximation of neighbour velocity adjustments used to engender the pressure equation and thus the velocity update. As a result, there is no desideratum to relinquish the pressure field to ascertain stability [25].

2.2.4 SIMPLEC skewness correction

The SIMPLEC technique, which comes along with skewness correction feature enables ANSYS FLUENT to get a solution on a highly skewed mesh, categorically on topology with varied slopes and sharp edges in the model, in about the same amplitude of iterations as a more orthogonal mesh [26]. The approximate link between the correction of mass flux at the cell face and the difference of the pressure correction at the circumventing cells is rather rough for meshes with some degree of skewness.

2.3 Meshing and Boundary Conditions

Due to the complexity of the model, tetrahedral meshing was applied to the geometry using ANSYS Meshing as depicted in Figure 5. Unstructured Tetrahedral elements are used since it can be adapted to arbitrary geometries with high accuracy [27]. Different sizes of meshing were generated with the size function such as proximity and curvature enabled. The generated mesh had been assigned with the name selections as illustrated in Figure 6 to the boundary condition to be used later in ANSYS CFD-Post Process. Since VOF method is used, air and water were assigned to both primary and secondary phase respectively.

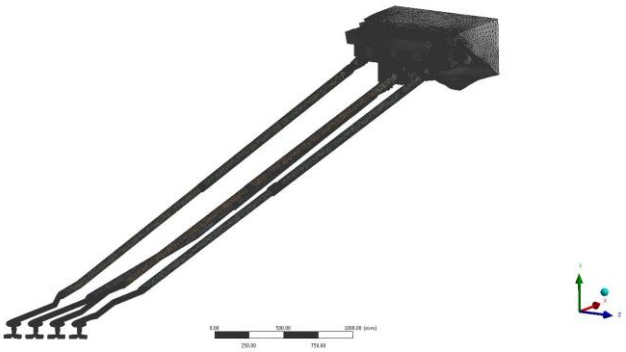

Fig. 5. Unstructured mesh on fluid domain

Fig. 6. Boundary conditions of fluid domain

Initial and boundary conditions are established for solution in order to control the flow's behavior and produce a distinct solution. The typical boundary conditions in this model are inlet, outlet, and wall symmetry.

i. Inlet. Under the Open Channel, the inlet was defined for Pressure Inlet boundary condition under the same group ID. The depth of the flow is kenned from advance from the experimental work which avails to define the Free-Surface Level (FSL) for the simulation afore-hand. The domain was then initialized under the volume fraction of the secondary phase (i.e., water) up to the FSL.
ii. Outlet. Pressure Outlet boundary condition is applied at the outlet. The pressure outlet boundary condition defines an outflow condition predicated on the flow pressure (P) at the outlet. This is utilized since FSL was assigned at the inlet. Here the, outlets are kept with another group ID.
iii. Wall symmetry. The walls and interior of the domain are defined as fluid. For this, Standard Wall Function has been implemented which abbreviates computational time.

2.4 Modification in Intake Structure

In theory, a significant number of operational problems may be avoided and better flow conditions might be achieved by making small adjustments close to the intake. One of the most affordable and popular ways to lessen the effects of air entrainment and swirl intensity is to employ anti-vortex plates. These plates can be used alone, in pairs, perpendicularly, obliquely, or even arced. As a result, the intake structure was modified, as shown in Figures 7 and 8, by enclosing intakes 1, 2, 3 and 4 with a fixed horizontal plate. At 30 mm above the intakes, two distinct plates—square and wedge—are positioned. These horizontal plates are meant to act as a buffer, slowing the formation of the swirl that gives rise to the vortex. Due to the frequent vortex formation at that level, the study will be conducted numerically at the minimum water level.

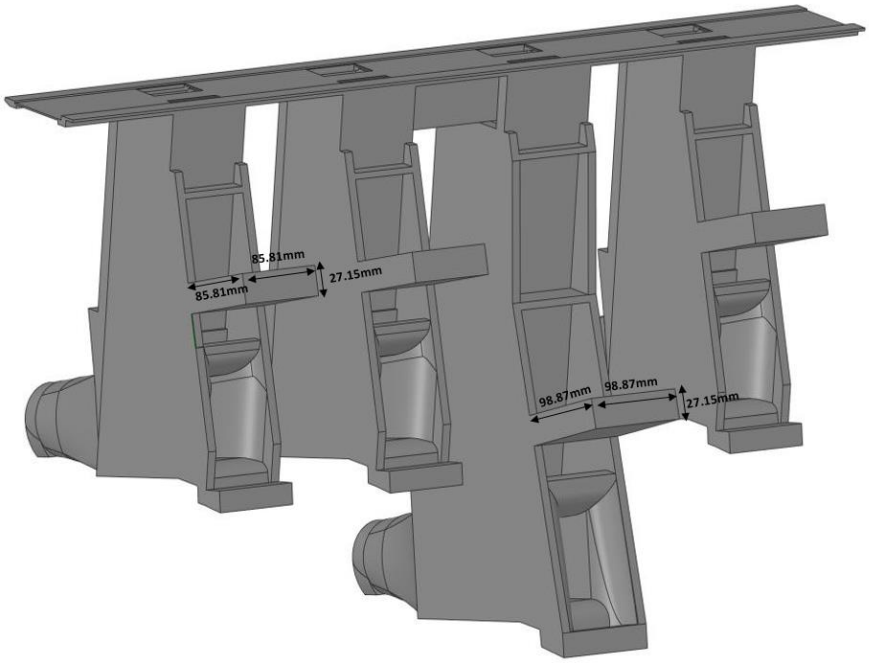

Fig. 7. Square-shaped plates

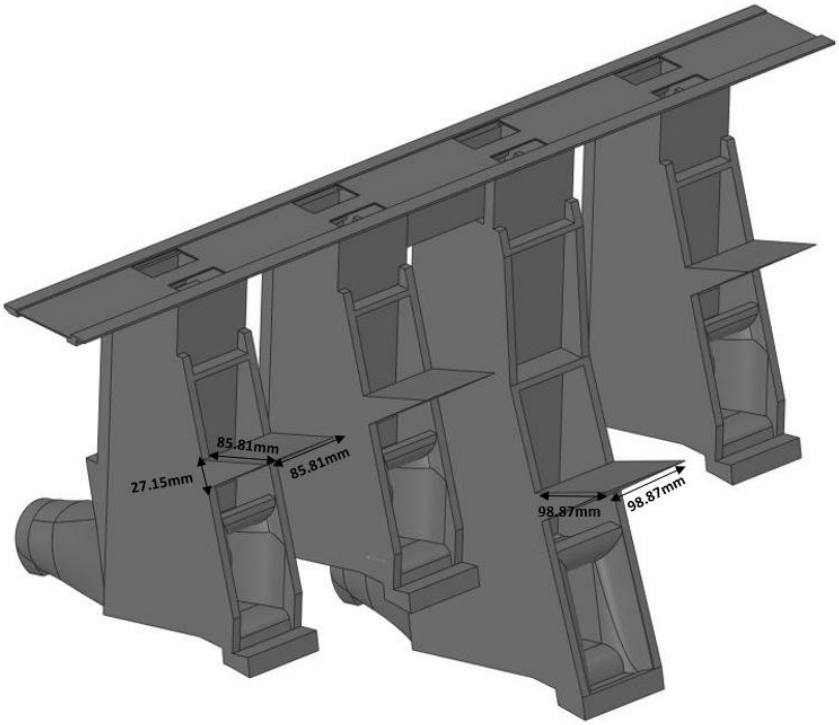

Fig. 8. Wedge-shaped plates

3. Results

3.1 Grid Dependency Test

The Grid Dependency Test is performed on three different mesh sizes, as shown in Table 1. Predicated on the examination of multiple grid conditions, the grid dependence test is a procedure used to determine the ideal grid condition without causing a difference in numerical results. By

comparing the CFD results for grid conditions culled at random for multiple grids of the model, the random sampling approach was utilised to identify the ideal grid [28]. This procedure was required to ensure that findings did not vary considerably as the number of cells increased, establishing a balance between accuracy and computing time. In this scenario, the mesh was reduced in size while all other parameters remained same. The mesh enhancement procedure has been completed to ensure that any future deviations in the mesh will not influence the estimated output [29]. The optimal grid was chosen based on the pressure outcomes from outlet 1 as depicted in Figure 9. The values are depicted in Figure 10.

Table 1
Mesh size with node and element number

Size (mm)	Node	Element
5.2	334083	1596917
5.1	336504	1699073
5.0	376826	1801229
4.9	403718	1929773
4.8	430610	2058316

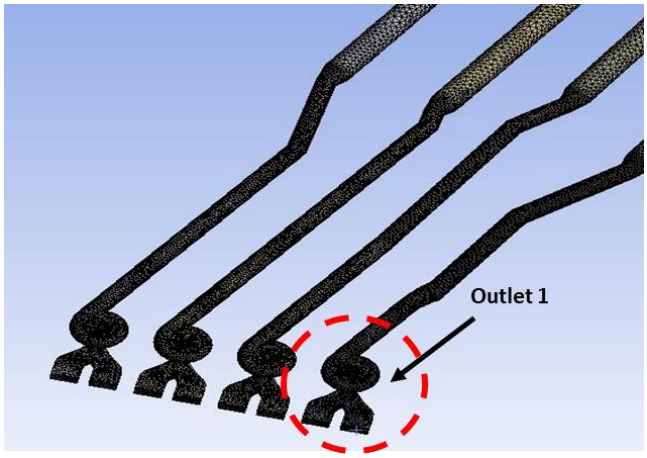

Fig. 9. Pressure Outlet 1

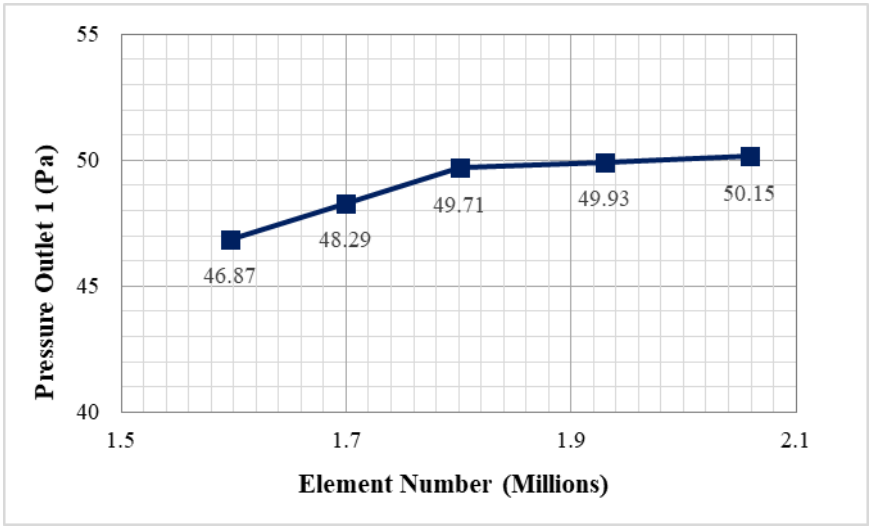

Fig. 10. Pressure versus Element size for Grid Dependency Test

According to Fig. 8, when the mesh element size is downsized from 5.2 mm to 4.8mm, the pressure values in outlet 1 have a little relevance in terms of discrepancies of roughly 6.5%. As a result, the model grid size of 4.8 mm was chosen since it provided acceptable accuracy.

3.2 Validation of Experimental and Numerical Model

Validation is accomplished by comparing CFD predictions to experimental data or real-world observations. In this situation, validation experiments were carried out on other similar hydraulic models for comparison [30]. Similar to the numerical model, a physical model was built in the hydraulic laboratory of the School of Civil Engineering at Universiti Sains Malaysia, the model scale ratios are displayed in Table 2. The velocity output from outlet 1, which is comparable, was used for both computational and experimental validation, as shown in Table 3. The Nixon Streamflo Velocity Meter was used to measure, indicate, and monitor extremely low water and other conductive fluid velocities.

Table 2
Scale ratio of model

Parameters	Scale
Length (m)	1:100
Velocity (m/s)	1:10
Discharge (m^3/s)	1:100000

Table 3
Velocity at outlet 1 for experimental and numerical

Water level (m) (Experimental/ CFD)	Experimental (m/s)	CFD(m/s)	Relative error (%)
0.34/2.428	1.67	1.62	3.0
0.38/2.485	1.98	1.70	14.1

The relative error among both prediction and measurement at recorded places was often considered as an essential trait in this study. The percentage discrepancy between velocity values at outlet 1 measured with a Nixon Streamflow Velocity meter and CFD is less than 20%, which is acceptable. The validation was allowed according to table 4 where A is less than 10%, B is between 10% and 20%, C is between 30% and 40%, and D is greater than 50%. Table 4 shows the accuracy quality for each category, beginning with A, which is deemed good, B, which is acceptable, C, which is minor, and D, which is low [31].

Table 4
Accuracy based on relative error

Category	Range (%)	Acceptability
A	<10	Good
B	<20-30	Acceptable
C	<30-40	Marginal
D	50>	Poor

3.3 Velocity Profile

The simulations are done on the minimum and maximum levels of the dam model, 2.428 m and 2.485 m (i.e., 0.34m and 0.38m from the experiment). Figure 11 and 12 depicts the predicted velocity flow field for each water level.

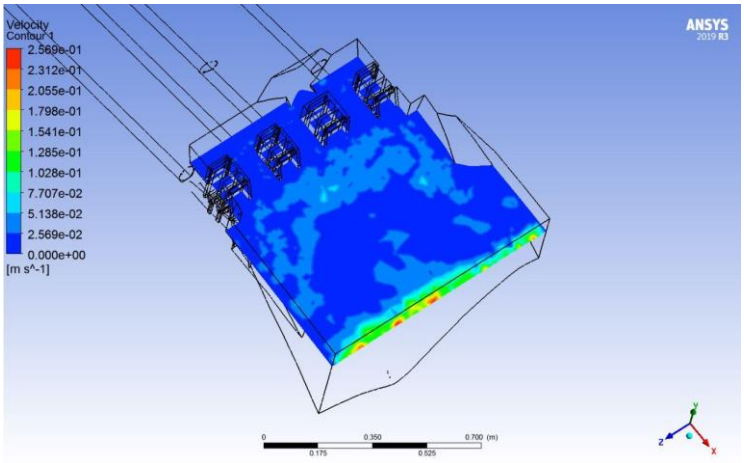

Fig. 11. Velocity Profile for 2.428m

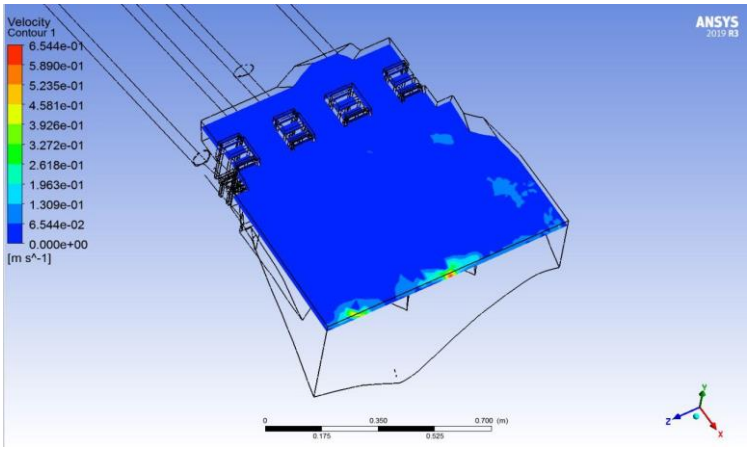

Fig. 12. Velocity Profile for 2.485m

It has been noted that the velocity at 2.428 m is highly turbulent in the reservoir's mid-region, as opposed to 2.485 m, where it appears to be relatively steady. This is because the water level of 2.428 m is more exposed to the surrounding topography. The flow velocity is affected by the form of the topology where friction is generated when water flows against the uneven and sharp edges of the ground. Furthermore, as time approaches the intake, water enters through intakes covered by smaller surrounding topology, causing the flow area at the entrance point to contract. This causes greater resistance to be met at the edges, where water molecules are slowed down, increasing the fluid speed in the intake area relative to the edges. The velocity in 2.485m is shown to be consistent in most areas, albeit it is significantly higher on the right side of the reservoir because of abrupt changes in flow direction that cause added turbulence, which is withal optically discerned in 2.428 m. Due to the inlet-outlet-velocity condition, which states that inflow velocity is dictated by the solution inside the domain and causes all inflow to be normal to the free boundary, the pressure inlets have been exhibiting the maximum velocity zone for both water levels.

3.4 Flow Profile before Modification

The simulations done on the minimum and maximum levels of the dam model, 2.428 m and 2.485 m have predicted the formation of free surface vortices. The predicted volume fraction for the secondary phase, or water, is depicted in Figures 13 and 14 for each water level. It appears that the reddish orange spots, which are the formation of vortices, are much more prevalent at the lowest

level. As was previously indicated, the formation of vortices or Free Surface Vortices (FSV) occurs rather often at minimal reservoir levels, and in this instance, which had a good agreement to the observations done at the experimental model. It is likely caused by unfavourable flow separation conditions close to the intake and sudden changes in flow direction at the right of the reservoir, which may be seen in both levels. Its high incoming flow velocity as in the velocity in the reservoir, $v\vartheta$, which is defined as the tangential velocity on an arbitrary location in the reservoir, may be used to observe the frequent vortex generation in 2.428m. Theoretically, increasing vortex tangential velocity results in a greater swirl flow [32]. Moreover, the reservoir's topology, intake design, and reservoir geometry all have an impact on the vortex's strength [33].

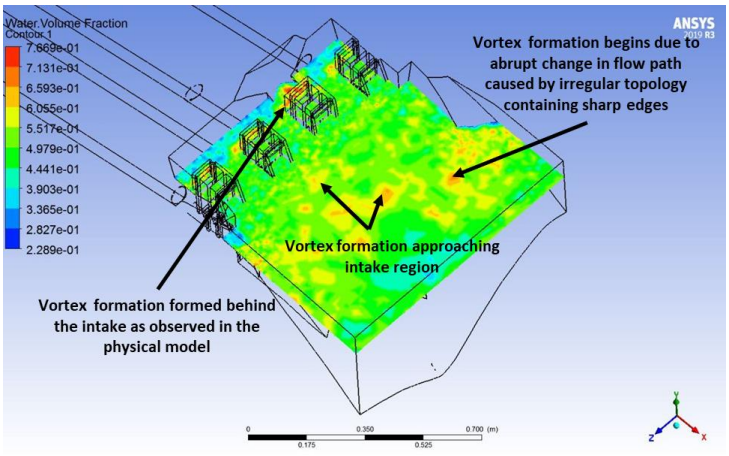

Fig. 13. Volume Fraction at 2.428m

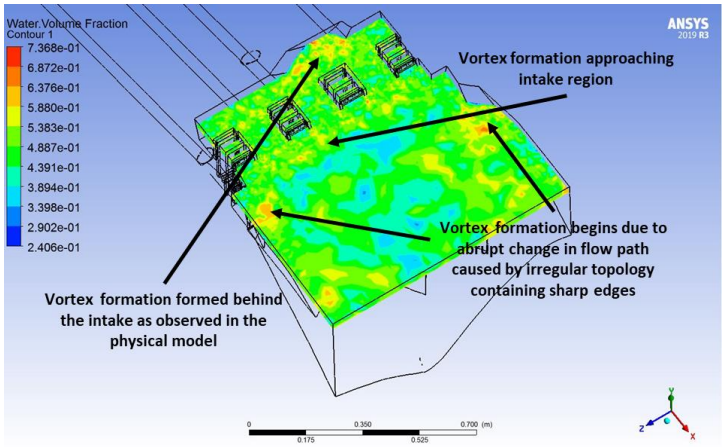

Fig. 14. Volume Fraction at 2.485m

3.5 Flow Profile after Modification

The simulations are done on the minimum and maximum level of the dam using both shapes square and wedge plates on the intakes. Figure 15 to 18 depicts the predicted volume fraction for the secondary phase of the after the modification.

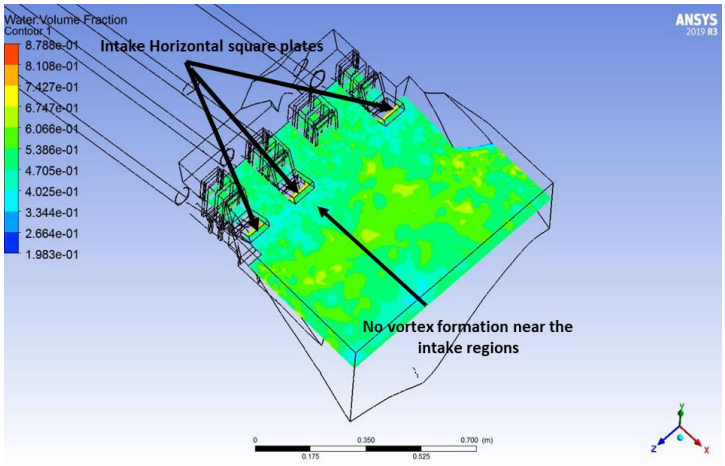

Fig. 15. Volume fraction for square-shaped plates at 2.428m

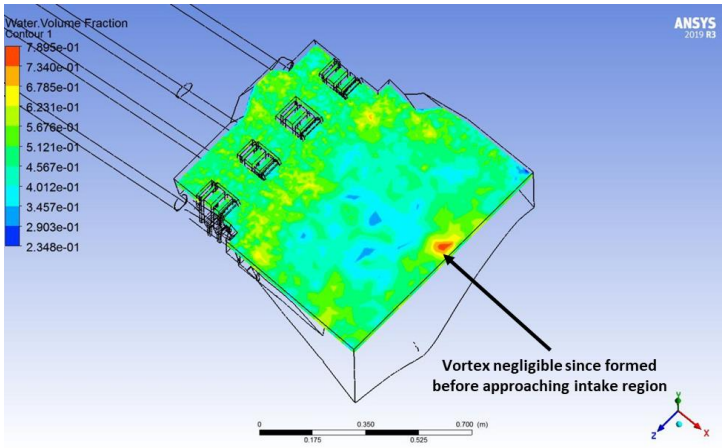

Fig. 16. Volume fraction for square-shaped plates at 2.485m

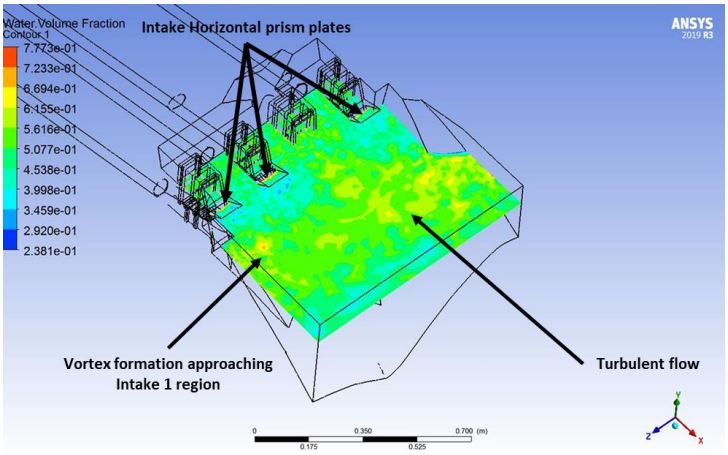

Fig. 17. Volume fraction for wedge-shaped plates at 2.428m

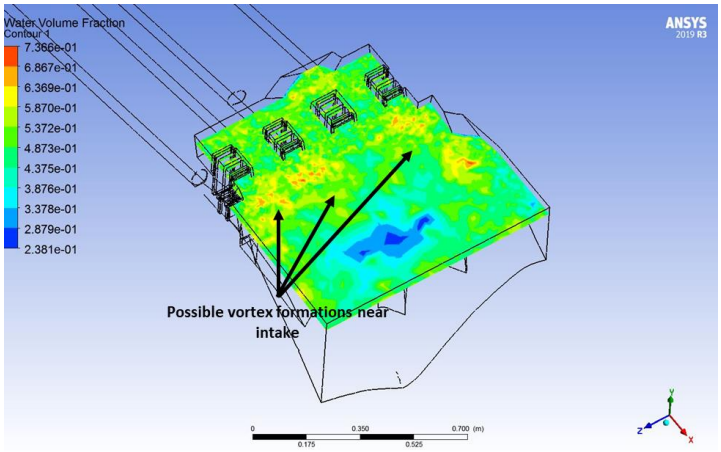

Fig. 18. Volume fraction for wedge-shaped plates at 2.485m

When a wedge plate is used instead of a square plate, the flow becomes more turbulent, according to the simulation. In other words, the square plates efficiently lower the speed of a rapid moving fluid and smooth it into a laminar flow rather than a turbulent flow, which has a beneficial effect on vortex class degradation. The degradation of the vortex core limits the vortex to a smaller class (Type 1 and 2) as well as the duration of the vortex formation. When wedge plates were utilised, vortex generation was seen around the Intake 1 region in both levels, implying that the swirling flow strength was not completely eliminated in the presence of the plates. As a result, the wedge plates have less influence on vortex class. Increasing the size of the wedge plates may lead the vortices to become unstable as well. Since the square plate's thickness is greater than that of a wedge, it appears to be considerably more able to minimize vortex strength than length at both levels. Additionally, it prevents vortices from trying to enter the intake from the sides.

4. Conclusions

A numerical analysis of a 3D dam reservoir model at two distinct water levels (2.428m and 2,458m) was performed. The VOF approach is used in numerical simulation to determine the flow characteristics of each level. Computed pressure values from outlet 1 from three different meshes are provided, and a grid dependence test is performed to find the best grid condition. This simulation is also useful for assessing hydraulic performance in terms of vortex mitigation before and after the installation of anti-vortex solid plates. When it comes to anti-vortex plates, square plates outperform wedge plates because square it lowers the speed of a fast-flowing fluid and reduces it into a laminar flow rather of a turbulent flow, which benefits vortex class deterioration. Based on validation comparisons of experimental and numerical velocity findings from this study's outlet 1, the data showed a significant agreement at water levels 2.428m and 2.458m, with relative errors of 3.0% and 14.1%, respectively. It also can be concluded that VOF-based CFD modelling may successfully be utilised to analyse open channel flows utilising 3D models with complicated topology if an appropriate computational mesh is built and appropriate boundary conditions are applied [34].

The circumscription from this numerical study is that simulation failure (i.e., floating point exception) is frequently caused by errors in the mesh structure due to high skewness. Highly skewed cells can decrease accuracy and destabilize the solution. The precision of the solution is significantly influenced by the mesh structure. The type of cell, the number of cells, and the simulation duration should all be carefully considered while carrying out precise solutions and delivering reliable findings. Before meshing, fixing the geometry to remove extraneous planes and edges can also assist to improve the skewness quality.

Acknowledgement

The authors would relish to thank Engineering Campus Universiti Sains Malaysia, (USM), Universiti Tenaga Nasional (UNITEN) and Tenaga Nasional Berhad (TNB) for its cooperation in consummating the project and conducting the research study. This research was not funded by any grant.

References

[1] Ho, David KH, K. M. Boyes, and Shane M. Donohoo. "Investigation of spillway behavior under increased maximum flood by computational fluid dynamics technique." In *14th Australasian Fluid Mechanics Conference, Adelaide University, Adelaide, Australia*. 2001.

[2] Zawawi, Mohd Hafiz, A. Saleha, A. Salwa, N. H. Hassan, Nazirul Mubin Zahari, Mohd Zakwan Ramli, and Zakaria Che Muda. "A review: Fundamentals of computational fluid dynamics (CFD)." In *AIP conference proceedings*, vol. 2030, no. 1, p. 020252. AIP Publishing LLC, 2018. https://doi.org/10.1063/1.5066893

[3] Mrope, Hamisi Ally, Yusufu Abeid Chande Jande, and Thomas T. Kivevele. "A Review on Computational Fluid Dynamics Applications in the Design and Optimization of Crossflow Hydro Turbines." *Journal of Renewable Energy* 2021 (2021): 1-13. https://doi.org/10.1155/2021/5570848

[4] Triwibowo, Bayu, Heni Wahyu Widayanti, and Miftakhul Indra Rukmanasari. "Prediction of Erotion Rate in Two Elbows for Coal-Air Flow Based on Computational Fluid Dynamics Simulation." *Journal of Advanced Research in Fluid Mechanics and Thermal Sciences* 97, no. 2 (2022): 115-125. https://doi.org/10.37934/arfmts.97.2.115125

[5] Zahari, Nazirul Mubin, Mohd Hafiz Zawawi, Fei Chong Ng, Mohamad Aizat Abas, Farah Nurhikmah, Nurhanani Abd Aziz, Lun Hao Tung, Iszmir Nazmi Ismail, Lariyah Mohd Sidek, and Mohd Rashid Mohd Radzi. "Finite Volume Method Numerical Modelling of the Penstock Flows in Dam Intake Sector Subjected to Varying Operating Conditions with Particle Image Velocimetry Validation." *Journal of Advanced Research in Fluid Mechanics and Thermal Sciences* 86, no. 1 (2021): 176-186. https://doi.org/10.37934/arfmts.86.1.176186

[6] Domfeh, Martin Kyereh, Samuel Gyamfi, Mark Amo-Boateng, Robert Andoh, Eric Antwi Ofosu, and Gavin Tabor. "Free surface vortices at hydropower intakes:–A state-of-the-art review." *Scientific African* 8 (2020): e00355. https://doi.org/10.1016/j.sciaf.2020.e00355

[7] Zahari, N. M., M. H. Zawawi, Fei Chong Ng, L. M. Sidek, Aizat Abas, F. Nurhikmah, Nurhanani A. Aziz, Tung Lun Hao, and M. R. M. Radzi. "Particle image velocimetry dynamic analysis on the penstock vortex flow for the dam reliability study." In *Resilient Infrastructure: Select Proceedings of VCDRR 2021*, pp. 493-501. Springer Singapore, 2022. https://doi.org/10.1007/978-981-16-6978-1_38

[8] Tahershamsi, Ahmad, Hassan Rahimzadeh, Morteza Monshizadeh, and Hamed Sarkardeh. "An experimental study on free surface vortex dynamics." *Meccanica* 53 (2018): 3269-3277. https://doi.org/10.1007/s11012-018-0878-3

[9] Azman, Aqil, N. M. Zahari, M. H. Zawawi, M. H. Mansor, F. C. Ng, Aizat Abas, F. Nurhikmah, and Nurhanani A. Aziz. "The Impact of Vortex Formation Due to The Operational Dam Condition: A Review." In *IOP Conference Series: Materials Science and Engineering*, vol. 920, no. 1, p. 012025. IOP Publishing, 2020. https://doi.org/10.1088/1757-899X/920/1/012025

[10] Möller, Georg, Martin Detert, and Robert M. Boes. "Vortex-induced air entrainment rates at intakes." *Journal of Hydraulic Engineering* 141, no. 11 (2015): 04015026. https://doi.org/10.1061/(ASCE)HY.1943-7900.0001036

[11] Walker, K. "Intake vortex formation and suppression at hydropower facilities." (2016).

[12] Amiri, S. Mahdi, Amir Reza Zarrati, Reza Roshan, and Hamed Sarkardeh. "Surface vortex prevention at power intakes by horizontal plates." In *Proceedings of the Institution of Civil Engineers-Water Management*, vol. 164, no. 4, pp. 193-200. Thomas Telford Ltd, 2011. https://doi.org/10.1680/wama.1000009

[13] Kabiri-Samani, A. R., and S. M. Borghei. "Effects of anti-vortex plates on air entrainment by free vortex." *Scientia Iranica* 20, no. 2 (2013): 251-258.

[14] Naderi, Vadoud, Davood Farsadizadeh, Ali Hosseinzadeh Dalir, and Hadi Arvanaghi. "Effect of using vertical plates on vertical intake on discharge coefficient." *Arabian Journal for Science and Engineering* 39 (2014): 8627-8633. https://doi.org/10.1007/s13369-014-1468-x

[15] Roshan, Reza, and Rasoul Ghobadian. "The Effect of Anti-Vortex Plates on Vortex Dissipation, Discharge Coefficient and Inlet Loss Coefficient in Hydropower Intakes." *Journal of Hydraulics* 17, no. 3 (2022): 15-29.

[16] Shrestha, Rakish, Samman Singh Pradhan, Prithivi Gurung, Amul Ghimire, and Sailesh Chitrakar. "A review on erosion and erosion induced vibrations in Francis turbine." In *IOP Conference Series: Earth and Environmental Science*, vol. 1037, no. 1, p. 012028. IOP Publishing, 2022. https://doi.org/10.1088/1755-1315/1037/1/012028

[17] Tey, Wah Yen, Yutaka Asako, Nor Azwadi Che Sidik, and Rui Zher Goh. "Governing equations in computational fluid dynamics: Derivations and a recent review." *Progress in Energy and Environment* 1 (2017): 1-19.

[18] Abouerraja, Lahcen, Hassan Samri, and Bennasser Bahrar. "Numerical Analysis of Transient Flow in Polyethylene Pipe." *Journal of Advanced Research in Fluid Mechanics and Thermal Sciences* 99, no. 2 (2022): 87-93. https://doi.org/10.37934/arfmts.99.2.8793

[19] Kumcu, Serife Yurdagul. "Investigation of flow over spillway modeling and comparison between experimental data and CFD analysis." *KSCE Journal of Civil Engineering* 21 (2017): 994-1003. https://doi.org/10.1007/s12205-016-1257-z

[20] Struyven, Florent, Zhenyi Guo, David F. Fletcher, Myeongsub Kim, Rosalinda Inguanta, Mathieu Sellier, and Philippe Mandin. "Suitability of the VOF Approach to Model an Electrogenerated Bubble with Marangoni Micro-Convection Flow." *Fluids* 7, no. 8 (2022): 262. https://doi.org/10.3390/fluids7080262

[21] Patel, T., and L. Gill. "Volume of fluid model applied to curved open channel flows." *WIT Transactions on Engineering Sciences* 52 (2006). https://doi.org/10.2495/AFM06036

[22] Khan, Umair, William Pao, Nabihah Sallih, and Farruk Hassan. "Flow Regime Identification in Gas-Liquid Two-Phase Flow in Horizontal Pipe by Deep Learning." *Journal of Advanced Research in Applied Sciences and Engineering Technology* 27, no. 1 (2022): 86-91. https://doi.org/10.37934/araset.27.1.8691

[23] Kaushik, Dinesh Kumar, and C. S. Nagendra. "CFD Analysis of Natural Convection Flow through Inclined Enclosure."

[24] Ahmed, Osman Abu Bakr Mohmmed, and Mark Ovinis. "Evaluation of k-epsilon model for turbulent buoyant jet." *Platform: A Journal of Engineering* 3, no. 2 (2019): 55-64.

[25] Aguerre, Horacio J., César M. Venier, César I. Pairetti, Santiago Márquez Damián, and Norberto M. Nigro. "A SIMPLE-based algorithm with enhanced velocity corrections: The COMPLEX method." *Computers & Fluids* 198 (2020): 104396. https://doi.org/10.1016/j.compfluid.2019.104396

[26] Moraes, A. D. O. S., P. Lage, G. Cunha, and L. F. L. R. da Silva. "Analysis of the non-orthogonality correction of finite volume discretization on unstructured meshes." In *Proceedings of the 22nd International Congress of Mechanical Engineering*, vol. 3, no. 7. 2013.

[27] Alfarawi, Suliman SS, Azeldin El-sawi, and Hossin Omar. "Exploring Discontinuous Meshing for CFD Modelling of Counter Flow Heat Exchanger." *Journal of Advanced Research in Numerical Heat Transfer* 5, no. 1 (2021): 26-34.

[28] Lee, Minhyung, Gwanyong Park, Changyoung Park, and Changmin Kim. "Improvement of grid independence test for computational fluid dynamics model of building based on grid resolution." *Advances in Civil Engineering* 2020 (2020): 1-11. https://doi.org/10.1155/2020/8827936

[29] Gupta, Durva, and Vaibhav Rai Khare. "Natural ventilation design: predicted and measured performance of a hostel building in composite climate of India." *Energy and Built Environment* 2, no. 1 (2021): 82-93. https://doi.org/10.1016/j.enbenv.2020.06.003

[30] Chesterton, Owen John, Mutlu Ucuncu, and Duncan Borman. "CFD modelling for dams and reservoirs–best practice workflows, specification and review." *Dams and Reservoirs* 29, no. 4 (2019): 148-157. https://doi.org/10.1680/jdare.19.00032

[31] Zhang, Zhao, Wei Zhang, Zhiqiang John Zhai, and Qingyan Yan Chen. "Evaluation of various turbulence models in predicting airflow and turbulence in enclosed environments by CFD: Part 2—Comparison with experimental data from literature." *Hvac&R Research* 13, no. 6 (2007): 871-886. https://doi.org/10.1080/10789669.2007.10391460

[32] Azarpira, Maryam, Hamed Sarkardeh, Sasan Tavakkol, Reza Roshan, and Hossein Bakhshi. "Vortices in dam reservoir: A case study of Karun III dam." *Sadhana* 39 (2014): 1201-1209. https://doi.org/10.1007/s12046-014-0252-7

[33] Roshan, R., H. Sarkardeh, and A. R. Zarrati. "Vortex study on a hydraulic model of Godar-e-Landar Dam and hydropower plant." *Computational Methods in Multiphase Flow V* 63 (2009): 217-225. https://doi.org/10.2495/MPF090191

[34] Oner, A. A., M. S. Akoz, M. S. Kirkgoz, and V. Gumus. "Experimental validation of volume of fluid method for a sluice gate flow." *Advances in Mechanical Engineering* 4 (2012): 461708. https://doi.org/10.1155/2012/461708